

Article

Numerical Heat Transfer Investigation in a Solar Receiver Heat Exchanger Channel with Punched Elliptical-Winglet Vortex Generators

Pitak Promthaisong^{1,a}, Pongjet Promvonge^{2,b}, Chitakorn Khanoknaiyakarn^{3,c}, and Sompol Skullong^{4,d,*}

¹ Heat Pipe and Thermal Tool Design Research Unit (HTDR), Faculty of Engineering, Mahasarakham University, Maha Sarakham 44150, Thailand

² Department of Mechanical Engineering, School of Engineering, King Mongkut's Institute of Technology Ladkrabang, Bangkok 10520, Thailand

³ Division of Mechanical and Automotive Engineering Technology, Faculty of Engineering and Technology, King Mongkut's University of Technology North Bangkok Rayong Campus, Rayong 21120, Thailand

⁴ Energy Systems Research Group and ATAE Research Unit, Department of Mechanical Engineering, Faculty of Engineering at Sriracha, Kasetsart University Sriracha Campus, 199 M.6, Sukhumvit Rd., Sriracha, Chonburi 20230, Thailand

E-mail: ^apitak.p@msu.ac.th, ^bkpongjet@gmail.com, ^cchitakorn09@gmail.com,

^{d,*}sompol@eng.src.ku.ac.th (Corresponding author)

Abstract. Thermal performance in a solar receiver heat exchanger (SRX) channel with punched elliptical-winglet vortex generator (P-EW) mounted on the absorber plate is numerically examined for Reynolds number (Re) ranging from 4000 to 24,000. In the present simulation, the P-EW characteristics included three ratios of winglet pitches ($P_R = 2.0, 1.5$ and 1.0) including four sizes of the perforated-holes (nondimensional hole diameter, $d_R = 0.0, 0.25, 0.417$ and 0.583) at one value of the attack angle ($\alpha = 30^\circ$) and relative height ($B_R = 0.48$). The computation reveals that employing P-EW generally yields considerably large friction factor (f) and Nusselt number (Nu) than the flat-plate channel alone. The use of smaller hole size causes the rise in Nu and f . It is noticeable that counter-spinning vortices pairs generated by the multiple P-EW can induce the impinging flow onto the absorber plate together with the air jet coming out of the hole, leading to the rise in the heat transfer rate greater than the smooth flat-plate channel. The highest thermal performance of about 1.9 was seen for the one with $P_R = 1.5$ and $d_R = 0.417$.

Keywords: Elliptical-winglet, heat exchanger, vortex generator, flow resistance, thermal performance.

ENGINEERING JOURNAL Volume 25 Issue 10

Received 5 May 2021

Accepted 10 October 2021

Published 31 October 2021

Online at <https://engj.org/>

DOI:10.4186/ej.2021.25.10.105

This article is based on the presentation at The 7th KKU International Engineering Conference 2021 (KKU-IENC 2021) at Khon Kaen University, Khon Kaen, Thailand, 12th-14th May 2021.

1. Introduction

Energy saving in a thermal system is one of the most important matter owing to the restriction of energy sources and production costs of such a system. Heat transfer augmentation (HTA) technology is a process of rising the heat transfer rate in the system and it can be classified as active and passive methods. These two methods are used in a diverse range of thermal system applications. A vortex flow device is one of the HTA techniques and has been widely applied in numerous industrial/engineering applications such as drying or curing of agricultural products, home warmth using solar air heater, thermal load cooling, heating process by air passing through the attic space of a house and so on. A heat exchanger is commonly employed as a component of thermal systems i.e., air conditioning, central heating and many uses in the chemical industry. Various vortex generator (VG) devices such as, coiled wire [1] twisted tape [2–4], conical and vortex rings [5, 6], baffle [7–12], fin [13], rib [14, 15], wing [16, 17], winglet [18–20] have been investigated to augment the heat transfer including thermal performance of such systems. VG devices are an important group of the passive HTA method in which the winglet-type vortex generator (WVG) shows the most important member of this group due to its low cost, easy production and installation. The WVG is designed to create a longitudinal vortex generator (LVG) along the heated surface of a heat exchanger. The LVG can help to thinner or disrupt the boundary layer near the wall and to raise the turbulence intensity leading to greater thermal performance, albeit with a minimal friction loss penalty. To date, most WVGs have been widely applied to improve the thermal performance of flat tube, fin-and-tube, channel/duct, and plate heat exchangers because of its advantage from low pressure loss and ease of manufacturing-and-installation in comparison with other VG devices.

Numerous experimental and numerical works have been carried out on maximizing the thermal performance by using the passive HTA techniques. Wu and Tao [21] numerically and experimentally examined the influence of location and spacing length of placing RWVG in a channel. Chompookham et al. [22] studied experimentally the pressure loss and heat transfer in a wedge-ribbed channel fitted with WVGs and found that the thermal performance was enhanced by 1.1–1.3. The effect of triangular ribbed channel combined with LVGs on thermal performance was experimentally investigated by Promvongse et al. [23]. Promvongse et al. [24] again studied the turbulent air flow and thermal behaviors in a ribbed channel combined with delta-winglet (DW) and showed that the DW having the attack angle of 30° has the best thermal performance. Skullong and Promvongse [25] experimentally explored the HTA in a channel with DWs and suggested that DW with $b/H = 0.4$, placed only on the absorber plate of the test channel yields the optimal thermal performance. Tang et al. [26] numerically studied the flow resistance and thermal characteristics in a

rectangular channel with two types of WVGs: RW and DW and revealed that the DW gives the highest overall thermal performance. Effects of dimples and their arrangement on the friction loss, heat transfer and flow structure in a SRX channel with DWVGs was numerically examined by Luo et al. [27] who indicated that the combination of dimples and DWVGs provides the thermohydraulic performance of about 1.46. Oneissi et al. [28] numerically investigated the heat transfer characteristics in a parallel plate-fin heat exchanger with two types of LVGs, delta winglet pair (DWP) and inclined projected winglet pair (IPWP). They showed that the IPWP with protrusions has the best thermal performance around 1.35. An effect of curved rectangular winglet vortex generator (RWVG) mounted in a channel on fluid flow structure as well as heat transfer behaviors was numerically studied by Naik et al. [29] who suggested that the curved RWVG has greater overall thermal performance than the plane RWVG due to stronger LVG and more disruption of the growth in the boundary layer. Skullong et al. [30] conducted a numerical and experimental work to explored the turbulent flow structure and thermal performance of a SRX duct using two perforated-winglet vortex generators, namely, perforated rectangular-and trapezoidal-winglet vortex generators (P-RWVG and P-TWVG). They pointed that P-TWVG yielded the best thermal performance. Effects of winglet height and longitudinal pitch of staggered rectangular winglet pairs was examined numerically by Bjerg et al. [31]. Han et al. [32] conducted a three-dimensional CFD simulation on flow and thermal characteristics in a fin-and-tube heat exchanger with arc winglet type vortex generators. A computation of thermal-hydraulic performance using DWs to produce LVG in a plain and wavy finned-tube heat exchanger was carried out by Xia et al. [33].

From the literature above, even though the WVGs have a definite confirmation in several types of heat exchangers with greater thermal performance, the finding of optimum WVG parameters to achieve an ideal thermohydraulic performance is still a challenge. Hence, the key purpose of the present work is to investigate numerically the thermal behaviors in a SRX channel with P-EWs placed repeatedly on the absorber plate. This work has never been studied previously. To obtain the optimal situation, the effect of diverse hole sizes on P-EWs on thermohydraulic performance is explored for Reynolds number between 4000 and 24,000.

2. Physical Model

2.1. Numerical P-EW Flow Model and Boundary Conditions

In a 3D computation for exploring the patterns of flow and thermal behaviors in a SRX channel fitted with P-EW, a periodical flow model with various hole sizes, ($d/b=d_R = 0, 0.25, 0.417$ and 0.583) and winglet pitch ratios, ($P/H=P_R=2.0, 1.5$ and 1.0) was numerically performed.

The elaboration of CFD work was explained as follows. In the computation, the finite volume approach was adopted in a 3D model simulation of periodically fully developed turbulent flow in a uniform heat-fluxed channel fitted with P-EWs. Assumptions of the flow model

included a steady turbulent incompressible flow, constant thermophysical properties of air, and neglecting the radiation and natural convection to the surrounding.

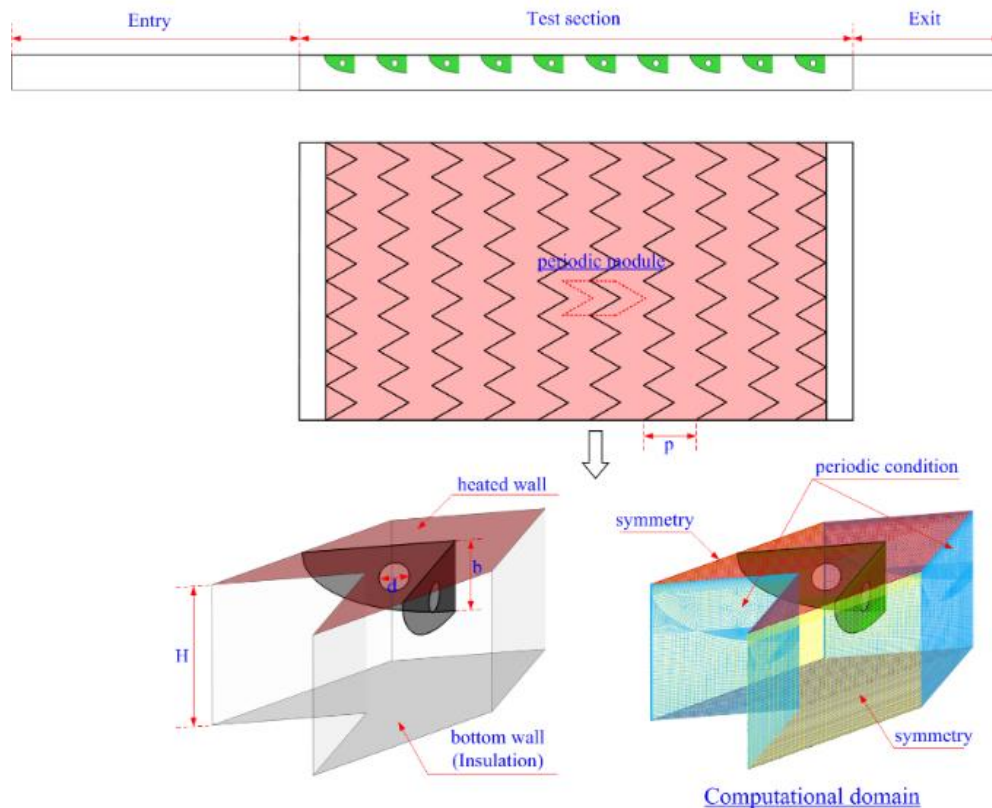


Fig. 1. P-EW configurations and computational flow domains.

Figure 1 shows the computation domain and the grid system of the present periodical-flow module. The pertinent characteristics and operating conditions were the channel width ($W=200\text{mm}$), the distance between upper and lower plates or channel height ($H=25\text{ mm}$), test channel ($L=800\text{mm}$) and the attack angle ($\alpha = 30^\circ$), transverse pitch spacing ($P_t=H$), relative winglet height ($B_R=b/H=0.48$) and pitch ratios ($P_R=P/H=2.0, 1.5$ and 1.0) and relative hole diameter ($d_R=d/b = 0, 0.25, 0.417$ and 0.583). The numerical flow model was performed for Re in a range of 4000 to 24,000 in line with the fully turbulent region. The governing equations of the flow field in the model was using the Reynolds average Navier-Stokes (RANS) as well as the equation of energy.

The finite volume method [34] was employed in discretizing the governing equations and linking the them by the QUICK scheme before numerically solving all the equations using the software, namely, ANSYS Fluent. The RNG $k-\varepsilon$ turbulent model was utilized with the SIMPLE algorithm for manipulating the coupling of velocity and pressure. The convergence criteria of the solutions were achieved once the residual values for all equations were beneath 10^{-6} excepting for the equation of energy under 10^{-9} . The detail of the boundary conditions and the computational domain is provided in Fig. 1. Because a

model of fully-developed periodical flow was assumed, just a single periodical flow module was employed. Two sides of the flow module were prescribed as symmetry planes whilst the inlet and outlet were set to periodic planes having a constant rate of mass air flow at 300 K, depending on the chosen value of Reynolds number. The test fluid was air whose properties remained constant throughout. All walls were set to impermeable and no-slip conditions and the enhanced wall treatment for the near-wall flow was used. A uniform 650 W/m^2 heat flux was utilized to the top plate whilst insulated surfaces were placed on the winglet and the lower plate. The rate of mass flow was estimated via Eq. (15) using Re as desired in a range of 4000 to 24,000. More details are provided in Ref. [9, 30].

2.2. Test of Grid Independence

Hexahedron elements were utilized in the current model of periodic flow. To verify the solution of grid independence, a procedure of the grid test was implemented with the four numbers of grid cells at about 105,645, 300,128, 502,005 and 705,506. It is noticeable that the changes of f and Nu at $Re=10,000$ are under 0.3% for increasing the amount of cell from 502,005 to 705,506,

as seen in Fig. 2. Hence, the rise in the cell number beyond this value has no advantage. Considering the convergence time and precise solution, the grid density at about 502,005 is adequate for the current computation.

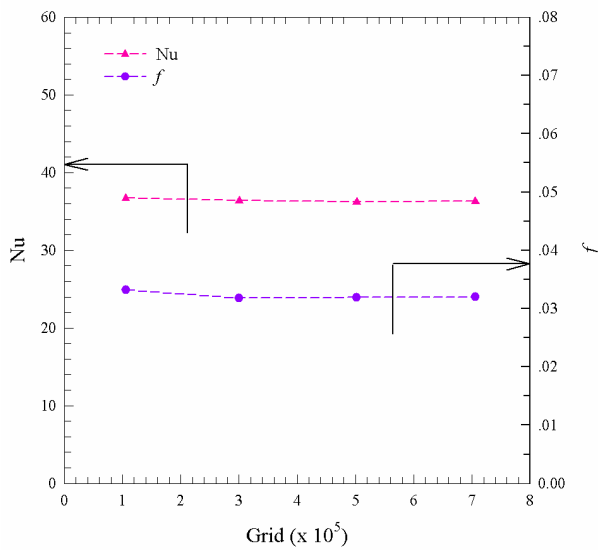


Fig. 2. Effect of grid density on Nu and f .

2.3. Pertinent Parameters in Simulation

The governing RANS equations as well as the energy equation are employed for this periodical flow model in common with the RNG k - ε turbulent model. In the form of a Cartesian tensor, these equations are expressed

Continuity:

$$\frac{\partial}{\partial x_i}(\rho u_i) = 0 \quad (1)$$

Momentum:

$$\frac{\partial}{\partial x_j}(\rho u_i u_j) = -\frac{\partial p}{\partial x_i} + \frac{\partial}{\partial x_j} \left[\mu \left(\frac{\partial u_i}{\partial x_j} - \overline{\rho u_i u_j} \right) \right] \quad (2)$$

in which ρ , p , u_i , u'_i and μ are, respectively, the density, pressure, mean velocity-component in the direction x_i , fluctuating velocity-component and absolute viscosity. The repeated indices mean the one to three summations for a three-dimensional flow problem.

Energy:

$$\frac{\partial}{\partial x_i}(\rho u_i T) = \frac{\partial}{\partial x_j} \left((\Gamma + \Gamma_t) \frac{\partial T}{\partial x_j} \right) \quad (3)$$

in which Γ_t and Γ are, respectively, turbulent and molecular thermal-diffusivities and both are denoted via

$$\Gamma_t = \mu_t / \text{Pr}_t, \text{ and } \Gamma = \mu / \text{Pr} \quad (4)$$

The term $(-\overline{\rho u_i u_j})$ appearing in Eq. (2) called Reynolds stresses, are modeled through the Boussinesq approach that links it to the gradients of mean velocities

$$-\overline{\rho u_i u_j} = \mu_t \left(\frac{\partial u_i}{\partial x_j} + \frac{\partial u_j}{\partial x_i} \right) - \frac{2}{3} \left(\rho k + \mu_t \frac{\partial u_i}{\partial x_j} \right) \delta_{ij} \quad (5)$$

in which the turbulence kinetic energy, k , is set as $k = \frac{1}{2} \overline{u_i u_i}$, δ_{ij} = Kronecker delta and the turbulent viscosity, μ_t is denoted as $\mu_t = \rho C_\mu k^2 / \varepsilon$. The RNG k - ε turbulence model is obtained from the Boussinesq approximation. By the RNG theory, their transport equations can be written as

$$\frac{\partial}{\partial x_i}(\rho k u_i) = \frac{\partial}{\partial x_j} \left(\alpha_k \mu_{eff} \frac{\partial k}{\partial x_j} \right) + G_k - \rho \varepsilon \quad (6)$$

$$\frac{\partial}{\partial x_i}(\rho \varepsilon u_i) = \frac{\partial}{\partial x_j} \left(\alpha_\varepsilon \mu_{eff} \frac{\partial \varepsilon}{\partial x_j} \right) + C_{1\varepsilon} \frac{\varepsilon}{k} G_k - C_{2\varepsilon} \rho \frac{\varepsilon^2}{k} - R_\varepsilon \quad (7)$$

where α_ε and α_k denote the inverse effective Prandtl numbers for ε and k , respectively whilst $C_{1\varepsilon}$ and $C_{2\varepsilon}$ are the constants. The term μ_{eff} is the effective viscosity and given by

$$\mu_{eff} = \mu + \mu_t = \mu + \rho C_\mu \frac{k^2}{\varepsilon} \quad (8)$$

where C_μ is set to 0.0845.

More detail on the mentioned model is reported in [9, 30]. Owing to the concept of a periodically fully-developed flow, a single periodical channel flow module is sufficiently modeled in the next computation.

Three parameters of interest include friction factor (f), Nusselt number (Nu), and thermal enhancement factor (TEF). The local Nusselt number (Nu_x) and the local convection coefficient (h_x) are evaluated by

$$h_x = q'' / (T_{s,x} - T_{m,a}) \quad (9)$$

$$Nu_x = h_x D_h / k_a$$

in which $T_{m,a}$ is the mean air temperature and $T_{s,x}$ is local surface temperature,

$$T_{s,x} = \frac{1}{A} \int_0^A T_s dA \quad (10)$$

where A and dA are, respectively, the surface and the differential areas of the absorber.

The average value of Nu is calculated by

$$Nu = \frac{1}{A} \int Nu_x dA \quad (11)$$

Re is the Reynolds number and is denoted as

$$Re = \frac{\rho \times U \times D_h}{\mu} \quad (12)$$

where the duct hydraulic diameter (D_h) is given as:

$$D_h = \frac{2 \times W \times H}{(W + H)} \quad (13)$$

Employing Δp across the periodic length of the module, L_p , f is computed from

$$f = \frac{(\Delta p / L_p) D_h}{\frac{1}{2} \rho U^2} \quad (14)$$

in which U is the average velocity of air.

The rate of mass flow is evaluated by

$$\dot{m} = \rho U A_c = \mu \text{Re}(H + W) / 2, \quad \dot{m}_{\text{module}} = \dot{m} / 8 \quad (15)$$

To judge the thermal performance by considering both the heat transfer and pressure loss at identical pump power, an indicator named thermal enhancement factor (TEF) as per Eq. (16), reported in [19, 36] is used:

$$\text{TEF} = \left(\frac{\text{Nu}}{\text{Nu}_0} \right)_{\text{Re}} \left/ \left(\frac{f}{f_0} \right)_{\text{Re}}^{0.755} \right. \quad (16)$$

where the subscript “0” stands for the smooth flat-plate channel only.

3. Validation

The simulated results from the present smooth flat channel using the RNG $k-\varepsilon$ turbulence model are introduced first and then compared to the results by the standard correlations of Dittus-Boelter and of Blasius [37], as given below.

Dittus-Boelter equation,

$$\text{Nu} = 0.023 \text{Re}^{0.8} \text{Pr}^{0.4} \quad \text{for heating} \quad (17)$$

Blasius equation,

$$f = 0.316 \text{Re}^{-0.25} \quad (18)$$

The numerical results of the current flat plate channel were validated with the results by the Dittus-Boelter correlation and the Blasius correlation [37], and those by Promvonge and Skullong [19] as portrayed in Fig. 2. It is noticeable that the Nu and f values of the present RNG $k-\varepsilon$ turbulence model are in reasonable agreement with experimental data and correlation's data. The deviations of Nu and f between the simulated and experimental data are less than $\pm 10\%$ each. Hence, this numerical validation is satisfactory for further simulation.

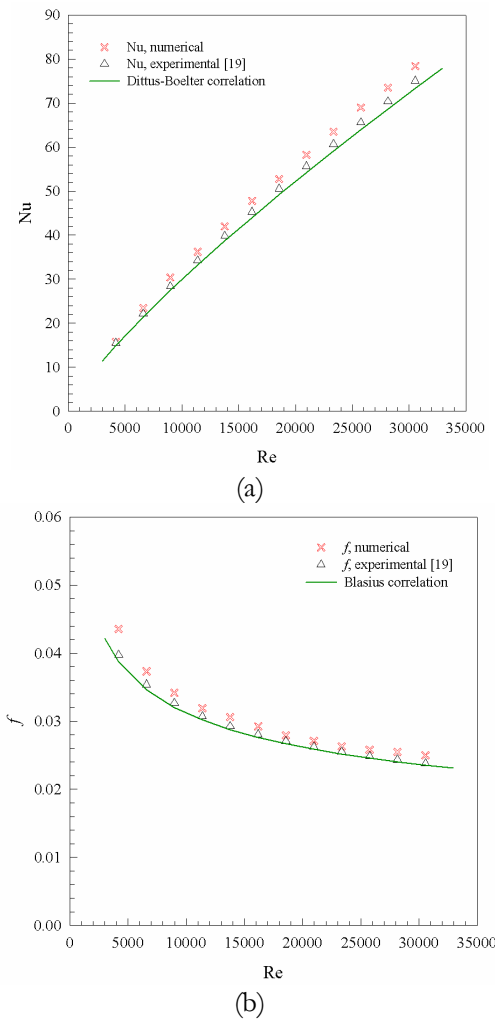


Fig. 2. Numerical validation for smooth flat-plate channel, (a) Nu and (b) f .

4. Numerical Results and Discussion

4.1. Heat Transfer

Influences of geometrical parameters of P-EW, including P_R ($= 1.0, 1.5$ and 2.0) and d_R ($= 0.583, 0.417, 0.25$ and 0) on the enhancement of the convection coefficient in terms of normalized Nusselt number (Nu/Nu_0) as well as Nusselt number (Nu) are portrayed in Fig. 3. In Fig. 3(a), displaying the effect of P-EW on Nu for $P_R = 1.0, 1.5, 2.0$ and $d_R = 0, 0.25, 0.417, 0.583$ with $\text{Re} = 4000-24,000$. It is seen that Nu tends to rise with increasing Re and has a greater value than the flat plate channel. It can be described that when Re rises, the velocity of fluid and the streamwise vortex strength are higher resulting in the greater augmentation in the rate of heat transfer. At a prescribed Re, Nu has an increasing trend with decreasing P_R and d_R owing to a stronger disturbance in the near wall region. The use of P-EW yields higher heat transfer of about 265–463 % than the flat plate channel.

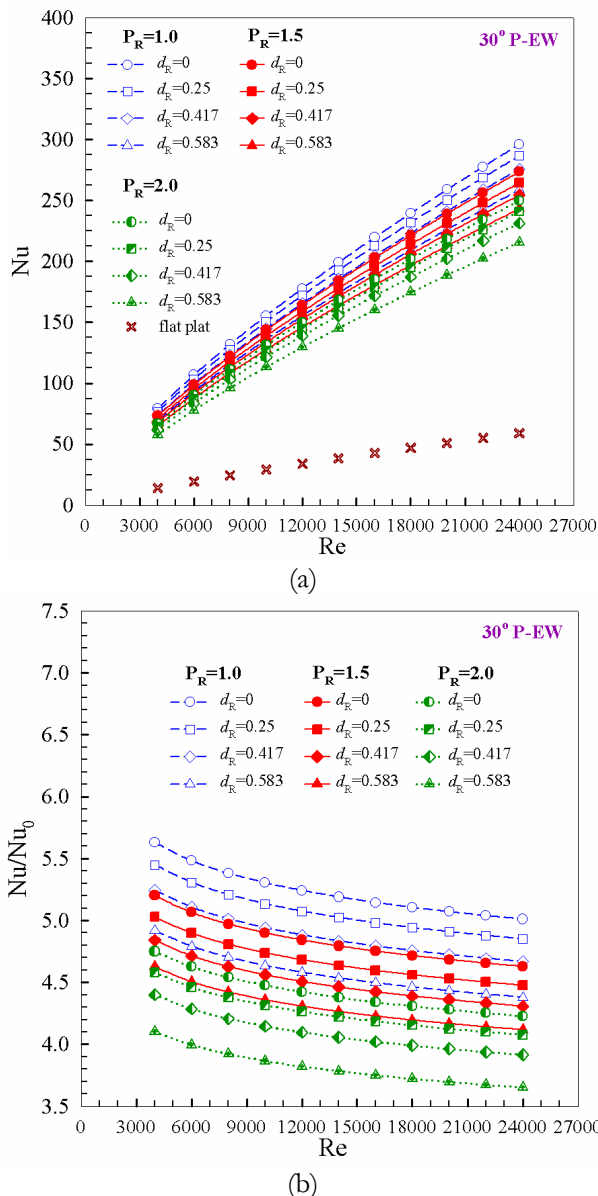


Fig. 3. Distributions of (a) Nu and (b) Nu/Nu₀ with Re for diverse P_R and d_R.

Figure 3(b) shows an effect of the varied Re on average Nu/Nu₀ for P-EW placed on the absorber. From the figure, it is manifest that Nu/Nu₀ tends to decline with rising Re. The Nu/Nu₀ values for P_R=1.0, 1.5 and 2.0 are, in average, around 5.23, 5.07, 4.88 and 4.58; 4.84, 4.68, 4.5 and 4.3; and 4.42, 4.26, 4.1 and 3.82 at d_R = 0, 0.25, 0.417 and 0.583, respectively. The Nu/Nu₀ has a maximum at about 5.63 for P_R = 1.0 and d_R = 0.

4.2. Flow Friction

As far as the effect of Re on f is concerned, Fig. 4(a) and (b) shows an effect of P_R and d_R on f and f/f_0 at various Re from 4000 to 24,000. It is noticeable that f has a flat change with rising Re or f is approximately free from Re whilst f increases with declining P_R and d_R. This maybe come from the dynamic pressure dissipation of fluid owing to greater surface area including the act from the reversing flow.

In Fig. 4(b), f/f_0 has a rising tendency with raising Re. The mean f/f_0 values for P_R=1.0, 1.5 and 2.0 are in a range of 79.96, 63.34, 53.72 and 44.18; 57.3, 45.36, 38.2 and 32.83; and 45.82, 35.21, 29.84 and 23.87 times at d_R = 0, 0.25, 0.417 and 0.583, respectively. This implies that the larger d_R, the lesser f/f_0 is. In other word, the use of punched hole on the winglet can reduce considerably the pressure loss in the SRX channel.

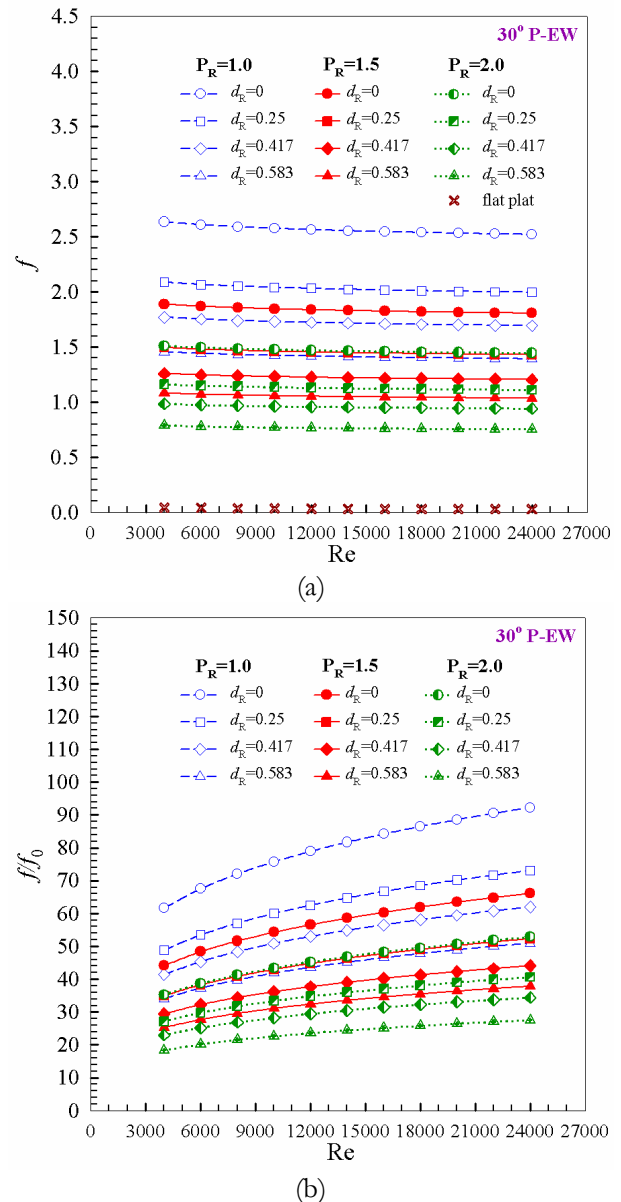


Fig. 4. Variations of (a) f and (b) f/f_0 with Re for various P_R and d_R.

4.3. Thermal Performance

Figure 5 displays the profile of TEF along with Re for different P_R and d_R. It is remarkable that TEF generally is higher than unity for all cases of P-EW, implying that the application of P-EWs in the SRX channel has benefit over the flat plate channel. Overall, TEF has the rising trend with decreasing Re. The TEF values for P_R=1.0, 1.5 and 2.0 are some 1.44–1.88, 1.46–1.9 and 1.42–1.85, respectively. From all the numerical data, it is clear that the employ of P_R = 1.5 and d_R = 0.417 leads to the best thermal

performance enhancement. The highest TEF for P-EW at $P_R = 1.5$ and $d_R = 0.417$ is found to be 1.9 at lower Re.

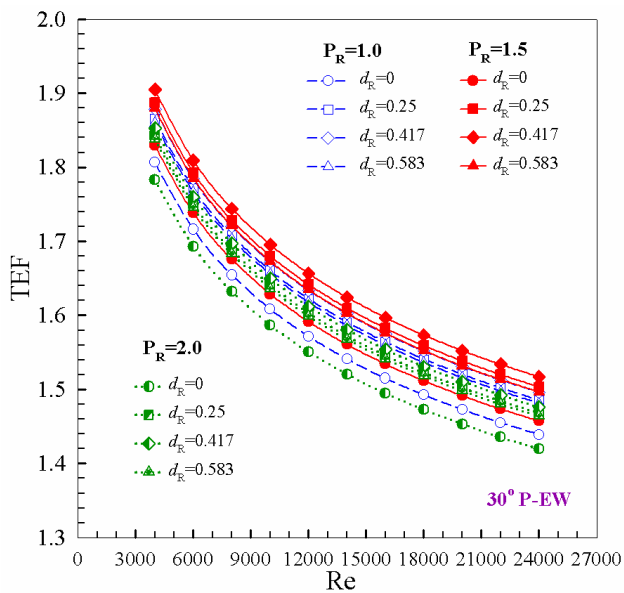


Fig. 5. Effect of P_R and d_R on TEF.

5. Flow Topologies and Heat Transfer Mechanism in SRX Channel with P-EWs

Streamlines and temperature contours of P-EW with $P_R = 1.5$ in the SRX channel have been examined for $d_R = 0$ and 0.417 . The contour plots at four plane locations were, respectively, portrayed in Fig. 6(a), (b) and (c) for using the smooth flat plate (Fig. 6(a)), the P-EWs at $d_R = 0$ (Fig. 6(b)) and at $d_R = 0.417$ (Fig. 6(c)). As found from the figure, the use of P-EW can produce pairs of counter-rotating vortices throughout the channel whilst there is no vortex for the case of the smooth flat channel, as expected (see Fig. 6(a)). The development of the boundary layer is destroyed from the placement of P-EWs on the absorber leading to the greater increase of the convection coefficient apart from exchanging heat between the core cold fluid and the wall hot fluid regions owing to the appearance of the counter-rotating vortices. This flow pattern provides the drastic increase in the heat transfer of the SRX channel, especially in the case of $d_R = 0$ winglet (see Fig. 6(b)).

The streamlines of the impinging-jet along the absorber for the P-EWs with $d_R = 0$ and $d_R = 0.417$ at $P_R = 1.5$, $Re = 10,000$ are presented in Fig. 7(a) and (b), respectively. As can be observed from the figure, the P-EW with $d_R = 0$ can induce efficiently the fluid to impinge upon the absorber plate due to stronger strength of the vortices while the one with $d_R = 0.417$ can also generate the counter-spinning vortices inducing the impinging jets on the absorber plate but lower strength of the vortices resulting from deteriorating the main vortices by the flow-jet coming out from the punched hole. However, the profit from using the P-EW is that the friction loss can be considerably decreased around 10 – 40 % while the heat

transfer is slightly reduced around 5 – 10% depending on the hole size.

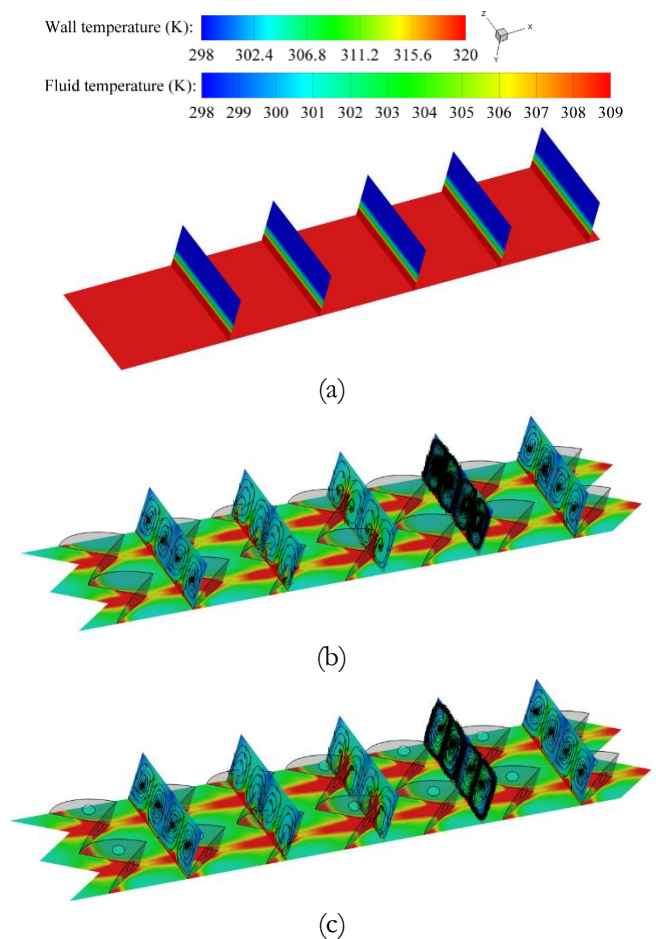


Fig. 6. Local wall temperature contours and fluid temperature fields with streamlines on transverse planes for (a) flat plate, (b) $d_R = 0$ and (c) $d_R = 0.417$ at $Re = 10,000$ and $P_R = 1.5$.

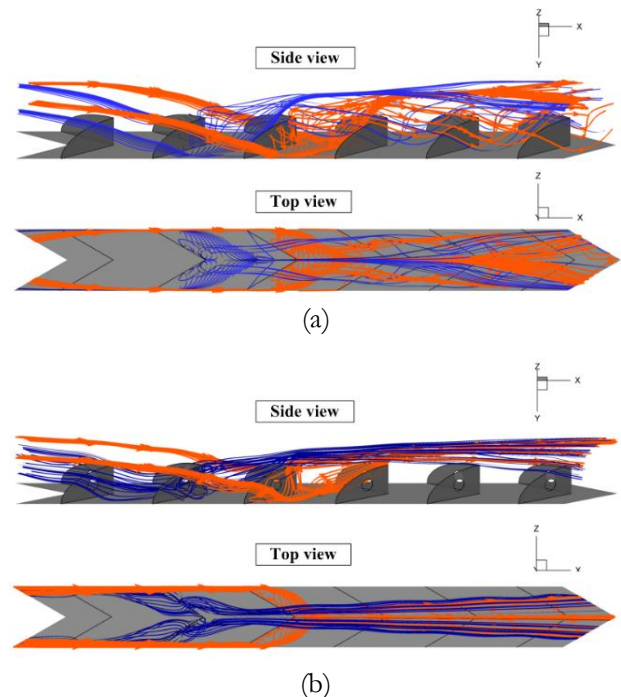


Fig. 7. Streamlines showing impinging-jet for P-EWs with (a) $d_R = 0$ and (b) $d_R = 0.417$, at $Re = 10,000$, $P_R = 1.5$.

Figure 8(a) and (b) shows the contour plots of jet-streamlines and the local Nusselt number on the absorber using the P-EWs with $d_R = 0$ and 0.417 at $Pr=1.5$, $Re = 10,000$, respectively. From the figure, it is noticeable that the larger Nu_x area (in red) appearing on the absorber wall with $d_R = 0$ can be observed whilst some smaller local Nusselt number area on the absorber with $d_R = 0.417$ can be visualized. The peak local Nusselt number area is noticed in the region of flow impingements behind the V-apex pointing upstream. This flow pattern implies that the P-EW yields greater heat transfer than the smooth flat channel alone.

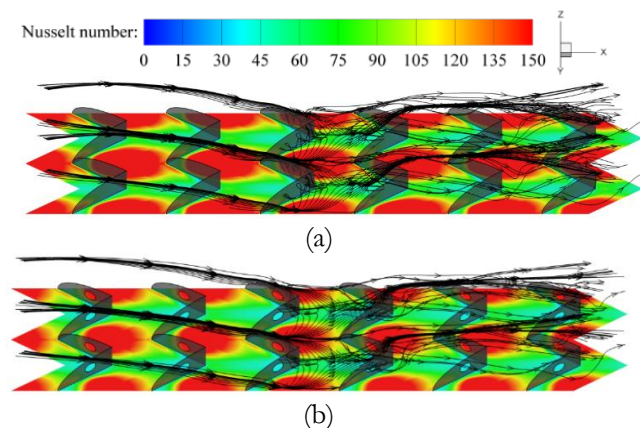


Fig. 8. Contours of local Nu_x and jet-streamlines for (a) $d_R = 0$ and (b) $d_R = 0.417$ at $Re = 10,000$, $Pr = 1.5$.

6. Conclusions

A numerical investigation of a SRX channel fitted with P-EWs has been conducted to study the influence of d_R and Pr on the thermohydraulic performance improvement for turbulent airflow, Reynolds number ranging from 4000 to 24,000. The P-EWs can generate the streamwise counter-rotating vortex pairs (SCVP) along the channel that help to induce the stronger impingement flows over the absorber plate, especially for $d_R = 0$. The key mechanism in enhancing the convection coefficient is mainly from the impinging-jet induction via the SCVP process. The existence of the solid winglet ($d_R = 0$) at $Pr=1$ provides a greater increase of pressure loss, $f/f_0 = 18.4 - 92.27$ but also gives a considerable heat transfer augmentation, $Nu/Nu_0 = 3.65 - 5.63$. The Nu and f have the uptrend with rising Re but with declining d_R for using the P-EW. The P-EW at $d_R = 0.417$ has the maximum TEF around 1.9 at lower Re where its optimum condition is at $Pr = 1.5$ and $d_R = 0.417$. Thus, the P-EW is considered as a prospective device for enhancing thermal performance of a SRX channel.

References

- [1] O. Keklikcioglu and V. Ozceyhan, "Entropy generation analysis for a circular tube with equilateral triangle cross sectioned coiled-wire inserts," *Energy*, vol. 139, pp. 65–75, 2017.
- [2] S. Chokphoemphun, M. Pimsarn, C. Thianpong, and P. Promvong, "Thermal performance of tubular heat exchanger with multiple twisted-tape inserts," *Chin. J. Chem. Eng.*, vol. 23, pp. 755–762, 2015.
- [3] S. Tamna, Y. Kaewkohkiat, S. Skullong, and P. Promvong, "Heat transfer enhancement in tubular heat exchanger with double V-ribbed twisted-tapes," *Case Stud. Therm. Eng.*, vol. 7, pp. 14–24, 2016.
- [4] S. Eiamsa-ard, C. Thianpong, and P. Promvong, "Experimental investigation of heat transfer and flow friction in a circular tube fitted with regularly spaced twisted tape elements," *Int. Commun. Heat Mass Transf.*, vol. 33, pp. 1225–1233, 2006.
- [5] M. E. Nakhchi and J. A. Esfahani, "Numerical investigation of different geometrical parameters of perforated conical rings on flow structure and heat transfer in heat exchangers," *Appl. Therm. Eng.*, vol. 156, pp. 494–505, 2019.
- [6] P. Promvong, N. Koolnapadol, M. Pimsarn, and C. Thianpong, "Thermal performance enhancement in a heat exchanger tube fitted with inclined vortex rings," *Appl. Therm. Eng.*, vol. 62, pp. 285–292, 2014.
- [7] P. Promvong, "Heat transfer and pressure drop in a channel with multiple 60° V-baffles," *Int. Commun. Heat Mass Transf.*, vol. 37, pp. 835–840, 2010.
- [8] P. Promvong and S. Kwankaomeng, "Periodic laminar flow and heat transfer in a channel with 45° staggered V-baffles," *Int. Commun. Heat Mass Transf.*, vol. 37, pp. 841–849, 2010.
- [9] S. Tamna, S. Skullong, C. Thianpong, and P. Promvong, "Heat transfer behaviors in a solar air heater channel with multiple V-baffle vortex generators," *Sol. Energy*, vol. 110, pp. 720–735, 2014.
- [10] P. Promvong, W. Jedsadaratanachai, S. Kwankaomeng, and C. Thianpong, "3D simulation of laminar flow and heat transfer in V-baffled square channel," *Int. Commun. Heat Mass Transf.*, vol. 39, pp. 85–93, 2012.
- [11] W. Jedsadaratanachai, N. Jayranaiwachira, and P. Promvong, "3D numerical study on flow structure and heat transfer in a circular tube with V-baffles," *Chin. J. Chem. Eng.*, vol. 23, pp. 342–349, 2015.
- [12] P. Promvong, S. Tamna, M. Pimsarn, and C. Thianpong, "Thermal characterization in a circular tube fitted with inclined horseshoe baffles," *Appl. Therm. Eng.*, vol. 75, pp. 1147–1155, 2015.
- [13] P. Promvong, S. Skullong, S. Kwankaomeng, and C. Thianpong, "Heat transfer in square duct fitted diagonally with angle-finned tape—Part 1: Experimental study," *Int. Commun. Heat Mass Transf.*, vol. 39, pp. 617–624, 2012.
- [14] S. Skullong, S. Kwankaomeng, C. Thianpong, and P. Promvong, "Thermal performance of turbulent flow in a solar air heater channel with rib-groove turbulators," *Int. Commun. Heat Mass Transf.*, vol. 50, pp. 34–43, 2014.

- [15] S. Skullong, "Performance enhancement in a solar air heater duct with inclined ribs mounted on the absorber," *J. Res. Appl. Mech. Eng.*, vol. 5, pp. 55–64, 2017.
- [16] S. Eiamsa-ard and P. Promvonge, "Influence of double-sided delta-wing tape insert with alternate-axes on flow and heat transfer characteristics in a heat exchanger tube," *Chin. J. Chem. Eng.*, vol. 19, pp. 410–423, 2011.
- [17] S. Skullong, P. Promvonge, C. Thianpong, and M. Pimsarn, "Thermal performance in solar air heater channel with combined wavy-groove and perforated-delta wing vortex generators," *Appl. Therm. Eng.*, vol. 100, pp. 611–620, 2016.
- [18] S. Skullong, P. Promvonge, C. Thianpong, N. Jayranaiwachira, and M. Pimsarn, "Heat transfer augmentation in a solar air heater channel with combined winglets and wavy grooves on absorber plate," *Appl. Therm. Eng.*, vol. 122, pp. 268–284, 2017.
- [19] P. Promvongea and S. Skullong, "Enhanced heat transfer in rectangular duct with punched winglets," *Chin. J. Chem. Eng.*, vol. 28, pp. 660–671, 2020.
- [20] S. Skullong, P. Promvonge, C. Thianpong, and M. Pimsarn, "Heat transfer and turbulent flow friction in a round tube with staggered-winglet perforated-tapes," *Int. J. Heat Mass Transf.*, vol. 95, pp. 230–242, 2016.
- [21] J. M. Wu and W. Q. Tao, "Numerical study on laminar convection heat transfer in a channel with longitudinal vortex generator part A: Verification of field synergy principle," *Int. J. Heat Mass Transf.*, vol. 51, pp. 1179–1191, 2008.
- [22] T. Chompookham, C. Thianpong, S. Kwankaomeng, and P. Promvonge, "Heat transfer augmentation in a wedge-ribbed channel using winglet vortex generators," *Int. Commun. Heat Mass Transf.*, vol. 37, pp. 163–169, 2010.
- [23] P. Promvonge, T. Chompookham, S. Kwankaomeng, and C. Thianpong, "Enhanced heat transfer in a triangular ribbed channel with longitudinal vortex generators," *Energy Convers. Manage.*, vol. 51, pp. 1242–1249, 2010.
- [24] P. Promvonge, C. Khanoknaiyakarn, S. Kwankaomeng, and C. Thianpong, "Thermal behavior in solar air heater channel fitted with combined rib and delta-winglet," *Int. Commun. Heat Mass Transf.*, vol. 38, pp. 749–756, 2011.
- [25] S. Skullong and P. Promvonge, "Experimental investigation on turbulent convection in solar air heater channel fitted with delta winglet vortex generator," *Chin. J. Chem. Eng.*, vol. 22, pp. 1–10, 2014.
- [26] L. H. Tang, W. X. Chu, N. Ahmed, and M. Zeng, "A new configuration of winglet longitudinal vortex generator to enhance heat transfer in a rectangular channel," *Appl. Therm. Eng.*, vol. 104, pp. 74–84, 2016.
- [27] L. Luo, F. Wen, L. Wang, B. Sundén, and S. Wang, "On the solar receiver thermal enhancement by using the dimple combined with delta winglet vortex generator," *Appl. Therm. Eng.*, vol. 111, pp. 586–598, 2017.
- [28] M. Oneissi, C. Habchi, S. Russeil, T. Lemenand, and D. Bougeard, "Heat transfer enhancement of inclined projected winglet pair vortex generators with protrusions," *Int. J. Therm. Sci.*, vol. 134, pp. 541–551, 2018.
- [29] H. Naik, S. Harikrishnan, and S. Tiwari, "Numerical investigations on heat transfer characteristics of curved rectangular winglet placed in a channel," *Int. J. Therm. Sci.*, vol. 129, pp. 489–503, 2018.
- [30] S. Skullong, P. Promthaisong, P. Promvonge, C. Thianpong, and M. Pimsarn, "Thermal performance in solar air heater with perforated-winglet-type vortex generator," *Sol. Energy*, vol. 170, pp. 1101–1117, 2018.
- [31] A. Bjerg, K. Christoffersen, H. Sørensen, and J. Hærvig, "Flow structures and heat transfer in repeating arrangements of staggered rectangular winglet pairs by Large Eddy Simulations: Effect of winglet height and longitudinal pitch distance," *Int. J. Heat Mass Transf.*, vol. 131, pp. 654–663, 2019.
- [32] H. Han, S. Wang, L. Sun, Y. Li, and S. Wang, "Numerical study of thermal and flow characteristics for a fin-and-tube heat exchanger with arc winglet type vortex generators," *Int. J. Refrig.*, vol. 98, pp. 61–69, 2019.
- [33] H. Ke, T. A. Khan, W. Li, Y. Lin, Z. Ke, H. Zhu, and Z. Zhang, "Thermal-hydraulic performance and optimization of attack angle of delta winglets in plain and wavy finned-tube heat exchangers," *Appl. Therm. Eng.*, vol. 150, pp. 1054–1065, 2019.
- [34] S. V. Patankar, *Numerical Heat Transfer and Fluid Flow*. New York: McGraw-Hill, 1980.
- [35] R. L. Webb, "Performance evaluation criteria for use of enhanced heat transfer surfaces in heat exchanger design," *Int. J. Heat Mass Transf.*, vol. 24, pp. 715–726, 1981.
- [36] P. Promvonge and S. Skullong, "Heat transfer in solar receiver heat exchanger with combined punched-V-ribs and chamfer-V-grooves," *Int. J. Heat Mass Transf.*, vol. 143, pp. 118486, 2019.
- [37] F. Incropera and P. D. Dewitt, *Introduction to Heat Transfer*, 5th ed. John Wiley & Sons Inc., 2006.



Pitak Promthaisong is currently a lecturer at Mahasarakham University, Thailand.

He received his D.Eng. (Mech. Eng.) from King Mongkut's Institute of Technology Ladkrabang (KMITL). His researches are in the area of heat transfer enhancement using computational fluid dynamic (CFD) and thermo-fluid under the Heat-Pipe and Thermal Tools Design Research Unit (HTDR).



Pongjet Promvonge obtained his Ph.D (Mech. Eng.) from Imperial College London, U.K. He is currently an Associate Professor of Mechanical Engineering at King Mongkut's Institute of Technology Ladkrabang (KMITL). His research areas emphasize on vortex-induced heat transfer, heat exchangers and thermal systems.



Chitakorn Khanoknaiyakarn is a lecturer at King Mongkut's University of Technology North Bangkok Rayong Campus, Thailand.

He obtained his D.Eng. (Mech. Eng.) from King Mongkut's Institute of Technology Ladkrabang (KMITL). His researches are in the field of heat transfer enhancement and thermal systems.



Sompol Skullong is currently an Associate Professor of Mechanical Engineering at Kasetsart University Sriracha Campus, Thailand.

He received his D.Eng (Mech. Eng.) from King Mongkut's Institute of Technology Ladkrabang (KMITL) in 2012. During his doctoral study period, he received the Royal Golden Jubilee (RGJ) scholarship from the Thailand Research Fund (TRF). His major researches currently focus on vortex/swirl flow in a heat exchanger tube, fluid mechanics, solar air heater, thermal systems and energy conservation.